A structure-and fabrication-informed strategy for the design of lattice structures with Injection 3D Concrete Printing

4 authors:

Yinan Xiao
Technische Universität Braunschweig
3 PUBLICATIONS   0 CITATIONS

SEE PROFILE

Shen Yuchi
Southeast University (China)
6 PUBLICATIONS   19 CITATIONS

SEE PROFILE

Norman Hack
Technische Universität Braunschweig
55 PUBLICATIONS   1,790 CITATIONS

SEE PROFILE

Pierluigi D'Acunto
Technische Universität München
58 PUBLICATIONS   269 CITATIONS

SEE PROFILE

Some of the authors of this publication are also working on these related projects:

Potential of additive manufacturing and performance in process comparison to conventional manufacturing in reinforced concrete construction. View project

Computational tools for creative structural design View project

A structure- and fabrication-informed strategy for the design of lattice structures with Injection 3D Concrete Printing

Yinan XIAO*, Yuchi SHEN[b], Norman HACK[a], Pierluigi D'ACUNTO[c]

* [a] Institute of Structural Design, Technische Universität Braunschweig
Pockelsstr. 4, 38104 Braunschweig, Germany
yinan.xiao@tu-braunschweig.de

[b] Department of Architecture, Southeast University
[c] Professorship of Structural Design, Technische Universität München

Abstract

This paper presents a design strategy that aims to integrate structural and manufacturing considerations in the conceptual design of three-dimensional lattice structures for Injection 3D Concrete Printing (I3DCP). Early experiments with I3DCP showed that multiple structural and fabrication constraints need to be taken into consideration in terms of node design. To address these constraints, a procedure for optimizing the geometry of the nodes of the designed lattice structures is introduced. Combined with 3D vector-based graphic statics, this approach provides intuitive visual information of the structural behavior both locally and globally. It allows controlling the internal forces within the target geometry. A case study of a pedestrian bridge is presented to test the proposed approach.

Keywords: 3D vector-based graphic statics, injection 3D concrete printing, structure- and fabrication-informed design, 3D convex hull, static rigidity of polyhedron, matrix analysis of lattice frameworks.

1. Introduction

Structural analysis and fabrication are typically treated as sequential steps after the conceptual design phase within the overall design process. This sequential approach, however, often leads to important modifications to the initial concept during the advanced design phase. Crucial information that appears during structural analysis and fabrication steps may force the whole procedure to turn back to the starting point, resulting in a redundant expense of time and resources [1]. Our work is motivated by the potential to integrate structure- and fabrication- informed strategies at the early phase of design to significantly improve the efficiency of the whole process from design to fabrication. The challenge is addressed and tested on a novel robotic additive manufacturing technique, Injection 3D Concrete Printing (I3DCP) [2].

By printing concrete into a non-hardening carrier liquid suspension [3], I3DCP overcomes the restrictions of conventional layered printing and gravitational forces, thus enabling the printing of intricate spatial concrete lattice structures (Fig. 1). In this approach, the print path can be aligned with complex spatial stress trajectories, which can be simply treated as strut-and-tie networks in the design phase. In comparison to conventional concrete printing methods, the range of variability in terms of printing angles is significantly expanded in I3DCP [3]. Recent work has already shown the benefits of this technique to print prototypes rapidly and precisely at small scales [3]. Yet, printing lattice structures via I3DCP can still be challenging due to several structural and fabrication constraints.
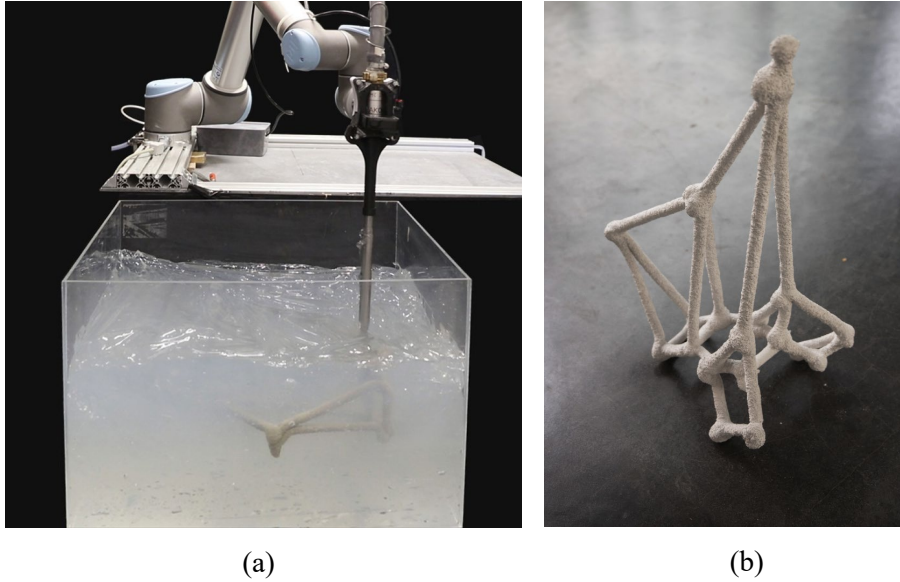
(a)   (b)

Figure 1: (a) I3DCP printing process with a UR10 robot; (b) A printed prototype.

1.1. Objective

The objective of this research is to develop a computational framework for the design of I3DCP lattice structures that integrates structure- and fabrication-informed constraints. The computational framework is built upon graphic statics, a geometry-based approach for the analysis and design of structures in static equilibrium [4]. Graphic statics relies on the form diagram to model the geometry of a structure with its applied loads, and the force diagram to represent the equilibrium of the forces applied to the nodes of the structure. In particular, the proposed computational framework takes advantage of Vector-based Graphic Statics (VGS) [5], a 3D graphic statics approach in which form and force diagrams are made out of vectors. In the proposed approach, the geometry of the original lattice structure is optimized to fulfill static requirements and match the goals for the fabrication. To this end, the constraints are categorized into two classes: topological and geometric constraints. The design process addresses the topological constraints first, and the geometric constraints afterward. By enforcing the interdependency between form and force diagrams via the VGS tool [6], the structure is kept in static equilibrium throughout the design process. Moreover, thanks to the visual perceptiveness of graphic statics [7], this approach allows for an intuitive understanding of the distribution of the internal forces in the designed structure. To validate the effectiveness of the proposed approach to real design scenarios for I3DCP, a pedestrian-bridge-prototype is used as a case study at the end of this paper. Similar projects that make use of graphic statics in combination with additive manufacturing for the design and construction of spatial lattice structures are, for example, the Digital Bamboo pavilion (2020) [8] and the Saltatur table (2020) [9].

1.2. Topological and geometric constraints of I3DCP

Based on preliminary printing experiments of concrete lattice structures with I3DCP, the following fabrication and structural constraints have been defined: (i) the maximum number of struts connected to the same node; (ii) the domain range of the angle between adjacent struts; (iii) the length domain of the struts; and (iv) the maximum magnitude of the internal forces in the struts according to the material properties and the length of the members. Valid lattice structures that can be fabricated using I3DCP should thus be designed to fulfill these constraints. However, based on the lattice structure design, several constraints may be incompatible and even in conflict with each other. For instance, Figure 2 shows an assembly of three equal edges as struts in compression under equilibrium carrying predefined loads. Assuming that nodes $\mathbf{V}_1$, $\mathbf{V}_2$, and $\mathbf{V}_3$ are constrained to fixed positions, only the position of node

V_0 can be freely adjusted along the line of action of the force F_0 that is applied to it. The domain of the edges' lengths ranges from L_{min} to L_{max} while the domain of the angle between adjacent edges is from α_{min} to α_{max}. The initial angle α between E_0 and E_1 is smaller than α_{min} and thus outside the allowable angle range. By moving the node V_0 to V_0', α changes to α' which is included within the allowable angle domain. However, at the same time the length of E_0 L_{E0} changes to $L_{E0'}$, which is shorter than L_{min}. As a result, modifying the position of node V_0 is not sufficient to satisfy both angle and length constraints simultaneously. Thus, a strategy of optimization to match the constraints individually is hardly suitable for the task at hand, and a more profound transformation of the node is required. In the proposed design approach for I3DCP lattice structures, constraints are categorized into two different classes (Table 1). The first class (*topological constraint*) concerns the topological relationship among the nodes and edges of the lattice structure regardless of the metric parameters; the second class (metric constraints) considers the metric parameters only.
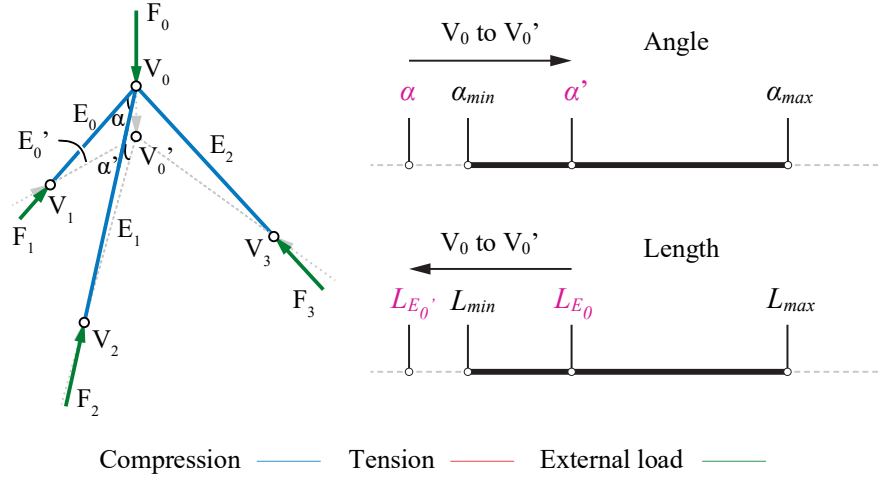

Figure 2: Three struts under equilibrium with incompatible constrains.

Table 1: The topological and metric constraints of I3DCP.

Topological constraint	Metric constraints				
Max node valence	Min edge length	Max edge length	Min angle between edges	Max angle between edges	Max internal force to critical buckling load ratio
Vlc_{max}	L_{min} (m)	L_{max} (m)	α_{min} (°)	α_{max} (°)	$br_{max} = (P/P_{cr})_{max}$

2. Method

The proposed computational optimization process for I3DCP lattice structures consists of two main steps (Fig. 3) and it is implemented within the Rhino/Grasshopper parametric environment [10], [11]. In Step 1, the topological constraint related to the maximum node valence Vlc_{max} is considered. Since the motion of the printing nozzle causes turbulence in the suspension around the node each time it passes by, nodes with high valence (normally over 6) may result in an overall imprecise lattice geometry. To tackle this problem, nodes of the lattice structure with valence exceeding Vlc_{max} are replaced by statically rigid polyhedrons whose vertices fulfill the node valence constraints. To preserve the global equilibrium of the replaced nodes, the vertices of the polyhedrons are inserted along the edges concurring in the

replaced nodes. In Step 2, an optimization of the polyhedral geometry takes place. The internal forces of the skeletal polyhedrons are first calculated (Step 2a), and vector-based 3D form and force diagrams are generated. In I3DCP, structural elements are made of concrete, and thus, achieving a compression-only structure is usually the goal of this form-finding step. Then, the metric constraints are introduced while the polyhedral geometry is relaxed (Step 2b). Throughout this procedure, the global equilibrium of the node is preserved by letting the vertices of the polyhedrons move only along the edges concurring in the replaced nodes. Moreover, the parallelism between corresponding edges of form and force diagrams is enforced [12].
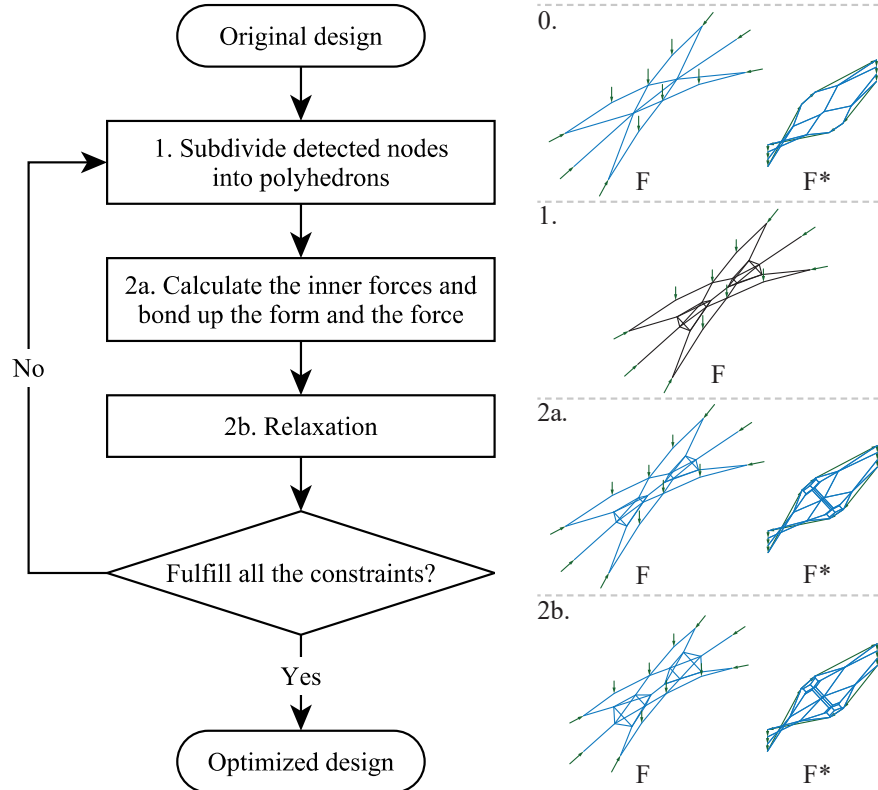

Figure 3: Left: flowchart describing the proposed computational optimization process for I3DCP lattice structures; right: design of a compression-only structure using the proposed method. (F is form diagram while F* is force diagram.)

2.1. Optimization of the topology

In I3DCP, the maximum node valence Vlc_{max} depends on the properties of different combinations of fine-grained concretes and carrier liquids into which the concrete is injected. The fresh concrete printed in the low yield stress carrier liquid has greater fluidity, making the printed edges easier to merge at the nodes. However, in this condition, the struts may have non-negligible bending deformation during the concrete hardening process, due to the lack of the bearing capacity of the carrier liquid (Fig. 4a). On the contrary, the carrier liquid with high yield stress may result in a better performance of straight struts (Fig. 4b). Nevertheless, merging the fresh concrete struts at the nodes will become more difficult since the concrete has to overcome the higher yield stress of the carrier liquid. The concrete recipe used in Figure 4 is the ready-mix Nafufill KM 250, MC Bauchemie with a maximum aggregate size of 4 mm. The dry-mixed compound is stirred with water in a mass ratio of 0.16 (water/ compound). The carrier liquid is a limestone suspension (Lhoist, d_{50} particle size of 5.9 μm) with a density of 1675 kg/m^3 in Figure 4a, and 1846 kg/m^3 in Figure 4b. Although the nodes in Figure 4a have a maximum of 12 valences

which is much higher than the 4-valent nodes in Figure 4b, the printed struts in Figure 4b have significantly better quality than Figure 4a.
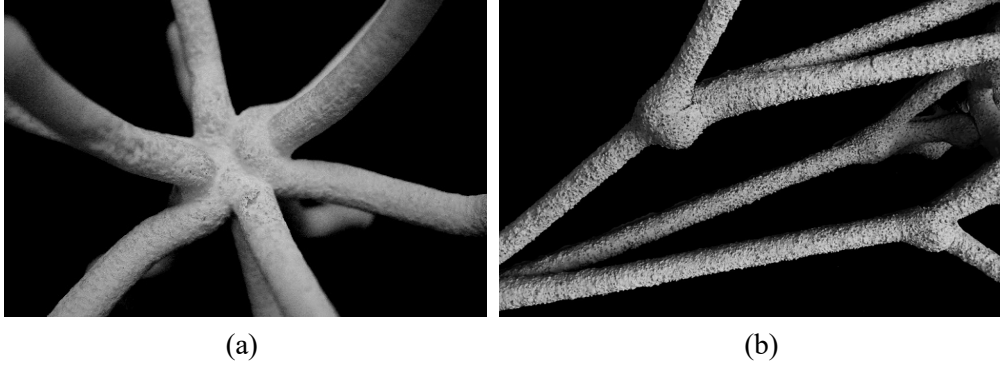

(a)   (b)

Figure 4: (a) A node printed in the carrier liquid with density of 1675 kg/m³. It is connected to 12 struts. Each pair of neighbor struts shares equal dihedral angle; (b) Nodes printed in the carrier liquid with density of 1846 kg/m³. It is connected to less but better-quality struts than Figure 4a.

2.1.1. Edge-node incidence matrix

In the conceptual design phase, the spatial lattice assemblies can be described as strut-and-tie networks with hinge joints. The relationship between nodes and edges can be represented by an edge-node incidence matrix C, consisting of the elements 1, or 0 in each row. The element C_{ij} is 1 if the edge $\mathbf{E}_i$ connects to the node $\mathbf{V}_j$. Otherwise, C_{ij} is 0. For example, the node of Fig. 1 can be described as:

$$C = \begin{matrix} V_0 & V_1 & V_2 & V_3 \\ \begin{bmatrix} 1 & 1 & 0 & 0 \\ 1 & 0 & 1 & 0 \\ 1 & 0 & 0 & 1 \end{bmatrix} & \begin{matrix} E_0 \\ E_1 \\ E_2 \end{matrix} \end{matrix} \tag{1}$$

Through this matrix, it is convenient to get corresponding information between nodes and edges. For example, the valence n_i of node $\mathbf{V}_i$ is given by left multiplication of an all-ones row vector $\boldsymbol{a}^T$ and C:

$$\boldsymbol{n} = \boldsymbol{a}^T C \tag{2}$$

For the assembly of Fig. 2, the valence n_i for each node is:

$$\boldsymbol{n} = \begin{bmatrix} 3 & 1 & 1 & 1 \end{bmatrix} \tag{3}$$

2.1.2. Static rigidity of lattice structure

Every node of the lattice structure that exceeds the maximum node valence Vlc_{max} is replaced by a statically rigid polyhedron connected to the same edges that concur into the original node. This newly generated polyhedron must follow two rules: 1) it must have the ability to resist the forces applied to the original node; and 2) the vertices of the polyhedron should satisfy the node valence constraint. As for the first rule, a statically rigid polyhedron is required to ensure that any applied forces can be redistributed while preserving the global equilibrium of the original node [13]. In this context, convex polyhedrons with only triangular faces (i.e. 3-valent faces) can be used as rigid spatial lattice structures [14]. Thus, a 3D convex hull with a Delaunay triangulation in space matches the requirements. For the second rule, the topology of the polyhedron should be defined so that the valence of its vertices does not exceed Vlc_{max}.

2.1.3. 3D convex hull

Figure 5a shows a node $\mathbf{P}$ connected to six other nodes, $\mathbf{P}_0$ to $\mathbf{P}_5$, through six edges. Assuming that the maximum node valence Vlc_{max} is 6, this node needs to be replaced by a statically equivalent polyhedron.

This polyhedron is generated as a Delaunay 3D convex hull whose vertices V_i (i = {0, 1 … 5}) are located on the edges E_i (i = {0, 1 … 5}). The process of formulating the 3D convex hull is based on the Quickhull algorithm [15]. These vertices can move along the six edges during the process. The newly created convex polyhedron c_0 is connected to the original global structure at the P_i nodes (Fig. 5b). However, not all the V_is are necessarily vertices of the convex hull. For instance, if V_2 moves to position V_2', it will end inside the convex hull and will be ignored in the newly generated cell c_1 (Fig. 5c). During the generating process of the 3D convex hull, the relative position between the current hull and the new added vertex V_i of the polyhedron can be determined by the dot product between the normal vectors of the faces of the polyhedron which keep directing outside, like n_{013} or n_{531}, and the vector from the vertex to any node that makes up the faces, such as $\overrightarrow{V_2V_0}$ or $\overrightarrow{V_2V_5}$. If the dot product value is positive, the vertex V_i is inside the current hull and will be ignored. Otherwise, the vertex V_i is outside and will be used to define the new 3D convex hull. According to the first rule (Section 2.1.2), all the V_i vertices of the polyhedron should be essential for generating the 3D convex hull since the external forces and edges around the node P have been predefined and the equilibrium condition should be maintained after the generation of the polyhedron.

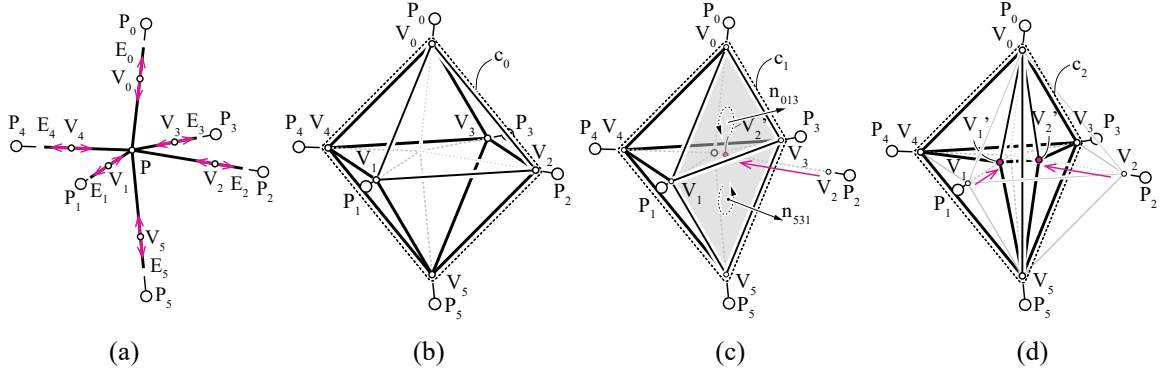Figure 5: (a) One node connected with six edges from the global structure; (b) A polyhedron with 5-valent vertices V_i generated as a convex hull on the vertices V_i; (c) Transformed polyhedron after moving V_2; (d) The nodes V_0 and V_5 become 6-valent in the polyhedron c_2.

2.1.4. Minimization of the valence of the polyhedral vertices

Adjusting the position of the vertices V_i along the edges E_i may change the valence of the vertices due to the reformulation of the convex hull geometry. This process is used to optimize the topological pattern of the generated polyhedron. To make sure that the polyhedral geometry respects the topological constraints and to facilitate the printing process, the valence of the polyhedral vertices is minimized. In the example (Fig. 5d), when the nodes V_1 and V_2 separately move towards V_1' and V_2', V_5 ends on the other side of the face $V_0V_1V_2$. Based on the definition of the convex hull, this results in the original polyhedron c_0 (Fig. 5b) becoming concave. Thus, to maintain the convex property, the edge V_1V_2 is replaced by a new edge V_0V_5, thus generating a new convex hull c_2. In c_2, the node valences of V_0 and V_5 change from 5 to 6, while that of V_1' and V_2' from 5 to 3. Assuming that Vlc_{max} is 5, c_0 is chosen instead of c_2. This optimization is implemented using the gradient-based Low-storage Broyden–Fletcher–Goldfarb–Shanno (LBFGS) algorithm [16] implemented in the NLOPT library [17].

2.2. Optimization of the geometry

After the topology of the polyhedron has been set, its geometry is adjusted to fulfill the metric constraints. This transformation modifies not only the edges' lengths and angles, but also their internal forces. Thanks to the VGS tool, it is possible to control these parameters simultaneously through the interdependent transformation of vector-based form and force diagrams [12].

2.2.1. Evaluation of the internal forces

When the nodes of the original structure that do not respect the node valence constraint have been replaced with polyhedrons, the force diagram of the original structure needs to be updated to reflect the new form. For each polyhedron, the forces on the extra edges connected to it are treated as external forces to this sub-structure. Since the polyhedron is a 3D convex hull with triangular faces, it is rigid and if it is connected to fixed nodes in space, the polyhedron is statically and kinematically determined [18]. Thus, the internal forces in the polyhedron can be calculated from the equation:

$$A \cdot f_E = f \qquad (4)$$

Where A is the equilibrium matrix, f_E is the vector representing the inner forces in the edges, and f is the vector of the external forces. To make sure the polyhedron is a fixed rigid body, six independent constraints should be added to the rigid body. A k ($k \geq 6$) × 6 kinematic matrix is applied to evaluate the constraints added to it, where k is the number of the constraints [18]. If six independent constraints achieve a global kinematically stable condition, then they can be treated as hypothetical unit edges connected to the supports of the polyhedron with fixed ends. The kinematic conditions of these six edges can consist of a block matrix A_e that adds to the right of the A in equation (4) and combine A as a new matrix $\tilde{A}$. The $\tilde{A}$ will be a square matrix with full rank because the polyhedron is now statically and kinematically determinate, which benefits the parse of f_E. The edited equation (4) becomes:

$$[A \quad A_e] \begin{bmatrix} f_E \\ f_e \end{bmatrix} = f \qquad (5)$$

Correspondingly, a vector f_e is added behind the vector f_E, representing the forces in the six hypothetical edges. Substituting the parameters of c_0 into equation (5) and results in equation (6):

$$
\begin{array}{c}
\begin{array}{cc} (E_{01}) & (E_{02}) \end{array} \quad \begin{array}{cccccc} (e_{ax}) & (e_{ay}) & (e_{az}) & (e_{bx}) & (e_{by}) & (e_{cz}) \end{array} \\
\left[
\begin{array}{ccccc}
\vdots & & \vdots & & \\
\cdots & \widehat{V_0 V_1}_x & \cdots & \widehat{V_0 V_2}_x & \cdots \\
\cdots & \widehat{V_0 V_1}_y & \cdots & \widehat{V_0 V_2}_y & \cdots \\
\cdots & \widehat{V_0 V_1}_z & \cdots & \widehat{V_0 V_2}_z & \cdots \\
& \vdots & & \vdots & \\
& \vdots & & \vdots & \\
& \vdots & & \vdots &
\end{array}
\right.
\left|
\begin{array}{cccccc}
\vdots & \vdots & \vdots & \vdots & \vdots & \vdots \\
0 & 0 & 0 & \hat{x} & 0 & 0 \\
0 & 0 & 0 & 0 & \hat{y} & 0 \\
0 & 0 & 0 & 0 & 0 & \hat{z} \\
\vdots & \vdots & \vdots & \vdots & \vdots & \vdots \\
\hat{x} & 0 & 0 & 0 & 0 & 0 \\
0 & \hat{y} & 0 & 0 & 0 & 0 \\
0 & 0 & \hat{z} & 0 & 0 & 0
\end{array}
\right]
\begin{bmatrix}
\vdots \\ f_{E_{01}} \\ \vdots \\ f_{E_{45}} \\ \vdots \\ \hline f_{e_{ax}} \\ f_{e_{ay}} \\ f_{e_{az}} \\ f_{e_{bx}} \\ f_{e_{by}} \\ f_{e_{cz}}
\end{bmatrix}
=
\begin{bmatrix}
\vdots \\ f_{V_0 x} \\ f_{V_0 y} \\ f_{V_0 z} \\ \vdots \\ \vdots
\end{bmatrix}
\end{array}
\qquad (6)
$$

In block A_e, the unit scalar numbers $\hat{x}, \hat{y}, \hat{z}$ describe the lengths of the six hypothetical edges. The six f_es represent the inner forces in them. By solving this formula, the inner forces in the edges of the polyhedron are attained. They can be added back to the original force list.

2.2.2. Translating nodes for compression-only strategy

In equation (6), when the f_{Eij} value is positive, it means the edge E_{ij} is under tension. If the value is negative, edge E_{ij} is under compression. By moving the nodes as described in section 2.1.3 but maintaining the topological structure in the polyhedron, the number of edges under tension can be reduced to zero under most circumstances. In the example of Figure 6a, after inner force analysis, the polyhedron c_0 contains one edge E_{12} under tension. Through adjusting the position of the polyhedral vertices V_i, a compression-only solution c_0' (Fig. 6b) is attained. Again, the process of finding the appropriate vertices position is applied with the NLOPT library [17]. However, there is the possibility that this operation may result in a concave polyhedron. Thus, the $\tilde{A}$ may become singular so that the

equation (5) has infinite or no solution. This situation should be ignored and kept on iterating until a full-rank situation.

2.2.3. Relaxation

After evaluating the magnitudes of the internal forces, vector-based form and force diagrams can be generated via the VGS tool. While keeping the interdependency between the two diagrams, the geometry of the structure can be then adjusted to fulfill the metric constraints. To this end, the Kangaroo2 solver is adopted [19]. Other than respecting the range of allowable edges' lengths and angles between adjacent edges, the designed structure must avoid buckling of the compression struts. Assuming that internal compression forces are perfectly aligned with the longitudinal axes of the printed struts, the maximum buckling ratio is defined as:

$$ br_{max} = \max\left(\frac{P}{P_{cr}}\right) \text{ with } P_{cr} = \frac{\pi^2 EI}{L^2} \tag{7} $$

where P is the actual compression force in the strut, P_{cr} is the critical buckling loads in the strut, E is Young's modulus, I is the moment of inertia of the cross-section, and L is the free length of the strut. The edges' length is displayed directly in the form diagram, while the inner force magnitudes are represented as lengths of the corresponded edges in the force diagram. They can be treated as parameters and substituted into the equation (7). This and the other metric constraints can be then embedded into the Kangaroo2 solver, each with a user-defined weight depending on the task at hand. Figure 6c illustrate the polyhedron c_0'' as resulting from the geometric transformation of c_0' after relaxation.
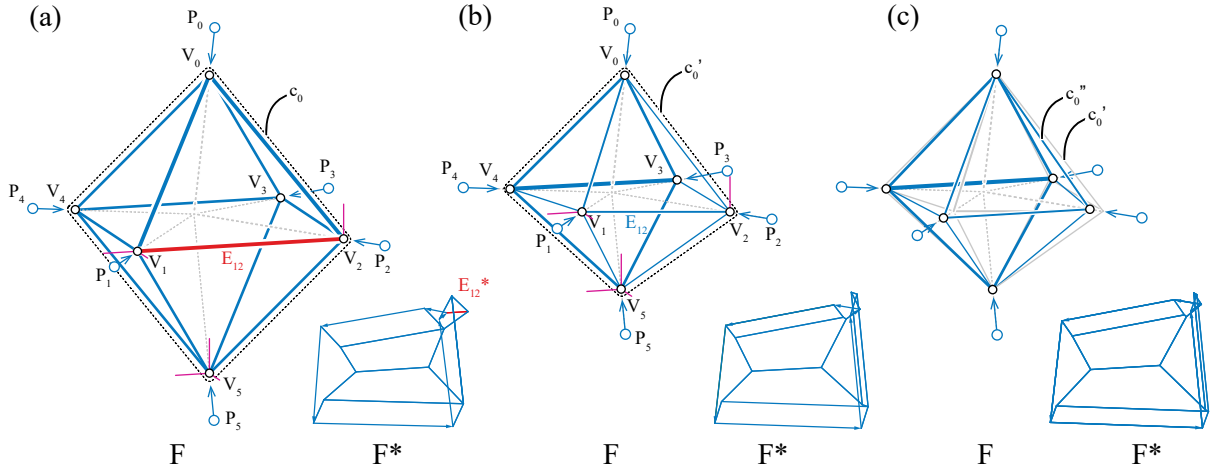

Figure 6: (a) The inner force solution for c0 polyhedron; (b) The compression-only solution as a new lattice of polyhedron c_0'; (c) The comparison between the c_0' and the one c_0'' after relaxation step. (The purple unit edges are hypothetical ones representing support constraints.)

3. Design case study – a compression-only concrete pedestrian bridge

To test the validity of the proposed approach, a pedestrian bridge has been designed to match the request of the I3DCP fabrication method. The original design is provided by Patrick Ole Ohlbrock (ETH Zurich) and Pierluigi D'Acunto (TU Munich) using the Combinatorial Equilibrium Modeling (CEM) tool [20]. The bridge spans 10 meters and is designed as a compression-only structure. To match the set-up of the small scale I3DCP on a UR10 robot, the bridge to be optimized here is a 1/5 scale model with a span of 2 meters (Fig. 7a). The force and form diagrams are generated with the VGS tool as inputs. The concrete and carrier liquid are set as the same as the one introduced in Section 2.1 (Fig. 4b). By the time of writing, the property of the concrete is still under ongoing investigation. The Young's modulus E of the concrete used for the design is around 3.0×10^4 N/mm^2, and it will be replaced according to the investigation result later. The diameter of the struts is set to 20 mm, which is equal to the inner diameter

of the printing nozzle. The predefined load for the bridge is 2.4 kN which is uniformly distributed to the top of it. The bridge is fixed to the ground with four supports on each end. According to Table 2, the original design has four 7-valent nodes, higher than the topological constraint. Figure 7b displays the result after the optimization of the topology step. Several internal forces on the struts of the newly generated polyhedrons are under tension, which results the structure to be edited for a compression-only solution. In addition, the length value L_{min} and maximum inner force over the crucial load $(P/P_{cr})_{max}$ are not satisfied as well. For these reasons, the design also needs to be adjusted to match the geometric request of I3DCP (Fig. 7c). The optimized result shown in Table 2 and Figure 8 satisfies the predefined constraints.

Table 2: Comparison between the original design of the bridge in Figure 7 and the design optimized to fulfill the constraints of I3DCP for the same materials described in Figure 4b.

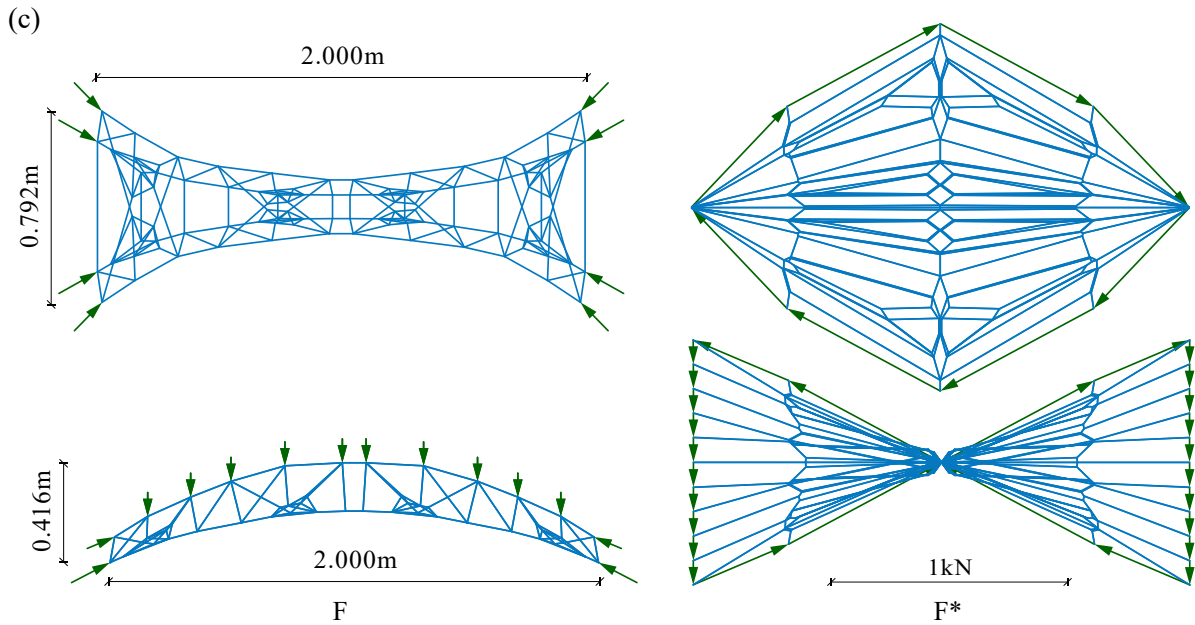|	Vlc_{max}	L_{min} (m)	L_{max} (m)	α_{min} (°)	α_{max} (°)	$(P/P_{cr})_{max}$
Constraints	6	0.050	0.600	15.0	180.0	1.000
Original design	7	0.040	0.570	16.0	178.2	1.391
Optimized design	6	0.061	0.539	16.8	179.0	0.976

(c)
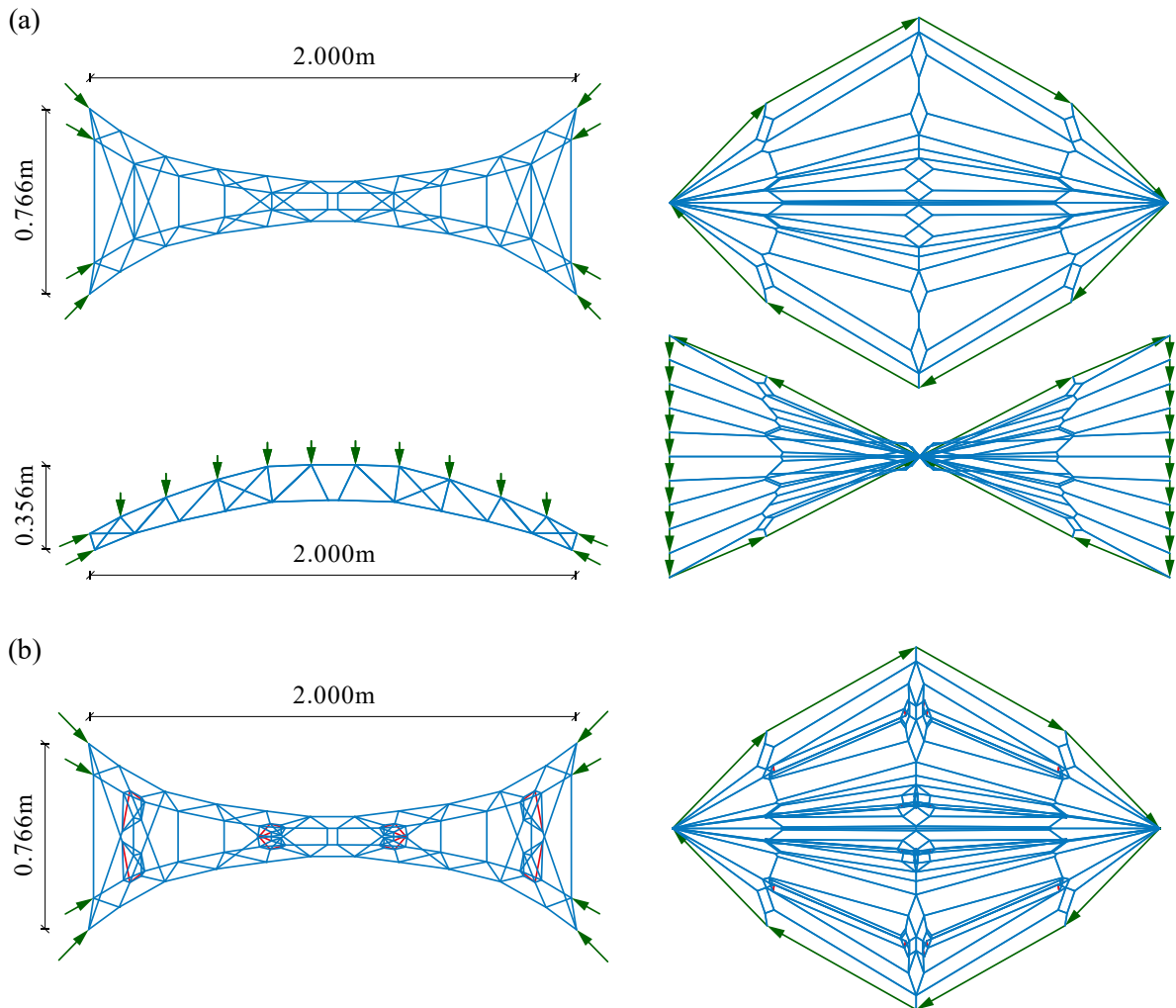
Figure 7: The top and side view of the form (F) and force (F*) diagrams of (a) the original pedestrian bridge; (b) The version after generating polyhedrons at the unqualified nodes; (c) The final version after relaxation.
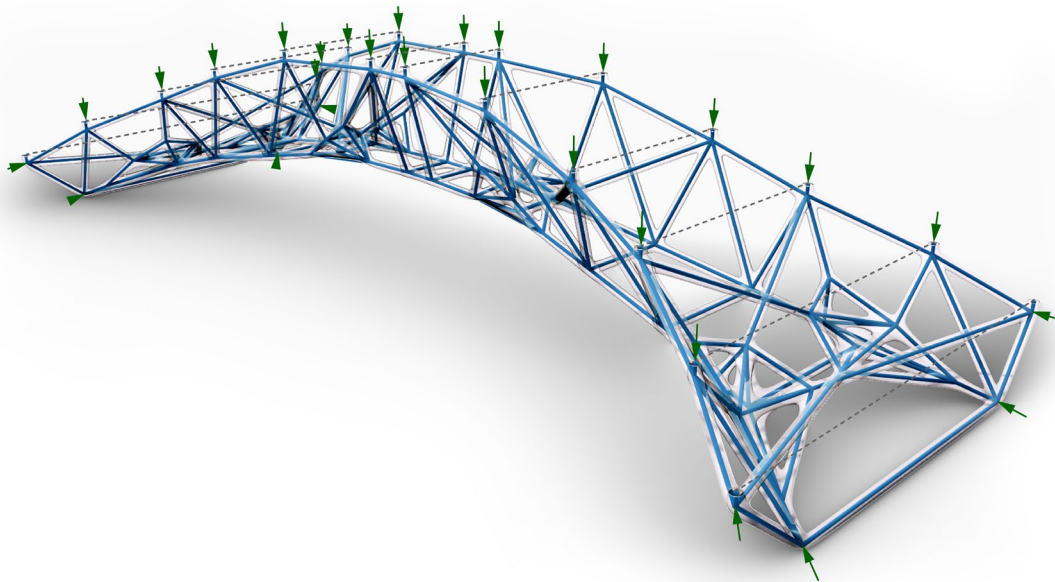

Figure 8: The perspective of the optimized version of the scaled pedestrian bridge.

4. Conclusion

This paper introduced a methodology for the Injection 3D Concrete Printing technique to generate reliable structures at the early design phase by combining the constraints that have been detected during the fabrication process and information gained from the structural analysis. A pedestrian bridge design has been optimized and tested to validate the approach. The bridge successfully fulfills the constraints that have been set for the optimization process and demonstrates the potential to apply the proposed approach to I3DCP.

In terms of the topological approach, further investigations will expand the range of sub-structures available to replace the high valent nodes, such as exploring different types of polyhedrons and fully utilizing the dual properties of the force diagram for the subdivision of the form. Concerning the geometrical aspects, more printing experiments will be carried out to tackle the fabrication constraints such as the distance between edges with the robot path planning.

Acknowledgments

References

[1]   A. J. Macdonald, *Structure and Architecture*, 2nd Editio. London: Routledge, 2001.

[2]   N. Hack, I. Dressler, L. Brohmann, S. Gantner, D. Lowke, and H. Kloft, "Injection 3D concrete printing (I3DCP): Basic principles and case studies," *Materials.*, vol. 13, no. 5, 2020, doi: 10.3390/ma13051093.

[3]   D. Lowke, A. Vandenberg, A. Pierre, A. Thomas, H. Kloft, and N. Hack, "Injection 3D concrete printing in a carrier liquid - Underlying physics and applications to lightweight space frame structures," *Cem. Concr. Compos.*, vol. 124, 2021, doi: 10.1016/j.cemconcomp.2021.104169.

[4]   M. Konstantatou, P. D'Acunto, and A. McRobie, "Polarities in structural analysis and design: n-dimensional graphic statics and structural transformations," *Int. J. Solids Struct.*, vol. 152–153, pp. 272–293, 2018, doi: 10.1016/j.ijsolstr.2018.07.003.

[5]   P. D'Acunto, J. P. Jasienski, P. O. Ohlbrock, C. Fivet, J. Schwartz, and D. Zastavni, "Vector-based 3D graphic statics: A framework for the design of spatial structures based on the relation between form and forces," *Int. J. Solids Struct.*, vol. 167, pp. 58–70, 2019, doi: 10.1016/j.ijsolstr.2019.02.008.

[6]   P. D'Acunto, Y. Shen, J. P. Jasienski and P. O. Ohlbrock, "VGS Tool - Vector-based Graphic Statics." 2021, [Online]. Available: https://github.com/pierluigidacunto/VGS.

[7]   T. Kotnik and P. D'Acunto, "Operative Diagramatology : Structural Folding for Architectural Design," *Des. Model. Symp. Berlin*, 2013.

[8]   D. Tanadini, P. O. Ohlbrock, M. Kladeftira, M. Leschok, E. Skevaki, B. Dillenburger and P. D'Acunto, "Exploring the potential of equilibrium-based methods in additive manufacturing: the Digital Bamboo Pavilion," in *Proceedings of IASS Annual Symposium*, 2022.

[9]   M. Akbarzadeh and A. T. Ghomi, "Saltatur," *Acadia 2020*, pp. 108–113, 2020.

[10] R. McNeel & Associates, "Rhinoceros." https://www.rhino3d.com/ (accessed Jun. 20, 2022).

[11] R. McNeel & Associates, "Grasshopper." https://www.grasshopper3d.com/ (accessed Jun. 20, 2022).

[12] P. D'Acunto, J. P. Jasienski, P. O. Ohlbrock, and C. Fivet, "Vector-Based 3D Graphic Statics: Transformations of Force Diagrams," in *Proceedings of IASS Annual Symposium*, 2017.

[13] P. D'Acunto, "Structural Folding for Architectural Design: A new approach to the design of folded plate structures in architecture," *PhD Thesis*, no. 25374, 2018.

[14] T. Wester, *Structural order in space : the Plate-Lattice dualism*. Copenhagen: Copenhagen : Plate Laboratory, Royal Academy of Arts, School of Architecture, 1984.

[15] C. B. Barber and D. P. Dobkin, "The Quickhull Algorithm for Convex Hulls," 1996.

[16] J. Nocedal, "Updating Quasi-Newton Matrices with Limited Storage," *Math. Comput.*, vol. 35, no. 151, p. 773, 1980, doi: 10.2307/2006193.

[17] S. Johnson, "The NLopt nonlinear-optimization package," 2022. http://ab-initio.mit.edu/nlopt.

[18] S. Pellegrino and C. R. Calladine, "Matrix analysis of statically and kinematically indeterminate frameworks," *Int. J. Solids Struct.*, vol. 22, no. 4, pp. 409–428, 1986, doi: 10.1016/0020-7683(86)90014-4.

[19] D. Piker, "Kangaroo: Form finding with computational physics," *Archit. Des.*, vol. 83, no. 2, pp. 136–137, 2013, doi: 10.1002/ad.1569.

[20] P. O. Ohlbrock and P. D'Acunto, "A Computer-Aided Approach to Equilibrium Design Based on Graphic Statics and Combinatorial Variations," *CAD Comput. Aided Des.*, vol. 121, p. 102802, 2020, doi: 10.1016/j.cad.2019.102802.